High-resolution spectra of 20-300 keV hard X-rays from electron precipitation over Antarctica

D. M. Smith,[1] R. P. Lin,[2] K. A. Anderson, K. Hurley, and C. M. Johns[3,4]

Space Sciences Laboratory, University of California, Berkeley

Abstract. In December 1990, a set of liquid-nitrogen-cooled germanium hard X-ray and gamma-ray spectrometers was flown aboard a high-altitude balloon from McMurdo, Antarctica, for solar, astrophysical, and terrestrial observations. This flight was the first circumnavigation ($\sim$9-day duration) of the Antarctic continent by a large (800,000-cubic-meter) balloon. Bremsstrahlung hard X-ray emission extending up to $\sim$300 keV, from the precipitation of high-energy electrons, was observed on six separate occasions over the auroral zone, all during low geomagnetic activity ($K_p \leq 2+$). All events were consistent with emission at the trapping boundary; observations over the polar cap showed no precipitation. We present the first high-resolution ($\Delta E \sim 2$ keV/full width at half maximum (FWHM) spectra of this hard X-ray emission in the energy range 20-300 keV. The observed count spectra are deconvolved by model-independent techniques to photon spectra and then to the precipitating electron spectra. The spectral hardness shows an inverse relation with L as expected. Our results suggest that high-resolution spectroscopy could be extremely effective in characterizing electron precipitation if coupled with imaging capability.

Introduction

Hard X-rays from the bremsstrahlung of magnetospheric electrons precipitating into the Earth's atmosphere were first observed at balloon altitudes by *Winkler et al.* [1958] over Minneapolis at times of strong magnetic disturbance. Subsequent balloon observations showed variable hard X-ray activity to be much more frequent over the auroral zone [e.g., *Anderson*, 1960; *Anderson and Enemark*, 1960; *Brown*, 1961], occurring $\gtrsim$ 50% of the time at invariant latitude 65°. The time-averaged count rate for this common X-ray "drizzle" is about 15 $(\text{cm}^2/\text{sec})^{-1}$, integrated above 25 keV [*Anderson*, 1965]. Below this energy the atmosphere above the balloon absorbs most of the X-rays. In intense precipitation events, fluxes ranging up to $\sim$200 $(\text{cm}^2/\text{sec})^{-1}$ have been seen [*Anderson and Enemark*, 1960; *Brown and Barcus*, 1963].

The hard X-ray spectrum drops off rapidly in energy, generally disappearing below background by $\sim$300 keV. The energetic electrons which create these hard X-rays

usually contain much less total energy than the softer (order of 1-10 keV) population of electrons responsible for visible aurorae.

Direct observations of precipitating electrons have been made by polar-orbiting satellites in low Earth orbit, as well as by satellites in high, equatorial orbits, sometimes simultaneously with balloon hard X-ray observations [e.g., *Parks*, 1970; *O'Brien*, 1962]. Polar-orbiting satellites, which sample many invariant latitudes over a long lifetime, have revealed statistical characteristics of auroral-zone precipitation, both by measuring precipitating electrons directly (distinguished by their pitch angle from trapped electrons) and by looking downwards to view hard X-ray bremsstrahlung emerging from the atmosphere [e.g., *Imhof et al.*, 1990].

From direct measurements on the Injun 3 satellite, electrons > 40 keV have been shown to be precipitating at values of L in the range 5-7 (essentially the auroral zone), and to appear sporadically at most other values of L as well, with intensities that vary over $\sim$5 orders of magnitude [*O'Brien et al.*, 1964]. Those data also showed that the precipitating flux per steradian sometimes approaches but never exceeds the flux of trapped electrons (i.e., the flux becomes nearly isotropic), and that this isotropy is less likely to be reached with higher energy.

From imaging of upward moving bremsstrahlung photons of energy 21 to 80 keV, it has been shown that auroral zone precipitation occurs over very broad arcs in longitude simultaneously [*Imhof et al.*, 1990]. The spectral hardness, flux and time structure of precipitation have a loose but complicated dependence on invariant latitude and local time [*Barcus and Rosenberg*, 1966]

and on local and global magnetic activity [*Anderson*, 1965] (see *Brown* [1966] for a summary of early results).

A principal goal of these studies has been to identify the origin of the precipitating particles. Early on, it was thought that they might originate directly from the trapped population, with their energy unchanged, dumped either by an adiabatic change in the Earth's magnetic field or by pitch angle scattering. The magnetosphere would be continually replenished by some steady source. It is now believed that the precipitating particles are freshly accelerated in the magnetosphere, due to two observations: (1) the rate of precipitation is often so high for so long at a given spot that the entire trapped population of the local flux tube would be depleted before new trapped flux could drift into the tube from other longitudes, and (2) when simultaneous measurements are made in the auroral zone and in the same flux tube at the equator, the trapped and precipitating fluxes are correlated, rather than anticorrelated, indicating a common and simultaneous source. These issues are discussed in depth by *Anderson and Enemark* [1960], *O'Brien* [1962], and *Parks* [1970], among others.

We describe the results of a 9-day circumpolar balloon flight over Antarctica, which sampled invariant latitudes from the auroral zone to the polar cap. Bremsstrahlung hard X-rays from 20 to 300 keV were observed from six electron precipitation events, all in the auroral zone. The high spectral resolution of these observations makes possible the application of a direct deconvolution technique to obtain the spectra of the X-ray-producing electron population, and then of the precipitating electron population. We discuss the spectral variations, threshold flux levels, and spatial pattern of the precipitation and compare the results to earlier observations.

Instrumentation

A large (~1130-kg) balloon payload was launched from Williams Field near McMurdo, Antarctica, on De-

cember 21, 1990. The balloon gondola, built at the Space Sciences Laboratory (SSL), University of California at Berkeley, carried three germanium spectrometer systems for high-resolution spectroscopy of solar, terrestrial, and astrophysical hard X-rays and gamma rays, in addition to several other experiments from other institutions.

One of the three spectrometer systems was an array of planar germanium detectors shielded by scintillator crystals in anticoincidence and collimated to view a narrow part of the sky. This system, intended specifically for astrophysical observations, did not detect precipitation activity at any time during the flight due to its small field of view. Each of the other two detector systems consisted of a single, closed-end coaxial germanium detector of approximately 5.5 cm in diameter and length (Fig. 1).

Each coaxial detector was electrically segmented along the inner bore such that energy depositions near the top of the detector were recorded on one electronics chain (front segment), and energy deposits in the rest of the detector were recorded on a second chain (rear segment). The segmentation in the first of these detectors was such that only the center of the front of the detector comprised the "front" channel, D0 (Fig. 1, left). This detector was flown with both segments, D0 and D1, open to the whole sky, with only a passive shield behind the detector to shield it from cosmic ray-produced hard X-rays from the atmosphere below. The front segment, D2, of the second detector contained the whole front surface, and that front segment was flown with a passive collimator and shield to view only the same small part of the sky as the planar array discussed above. As can be seen in Fig. 1, right, the rear segment of this detector, D3, was left open. It is D1, the rear segment of the first detector, (Fig. 1, left) which is used in the analysis below.

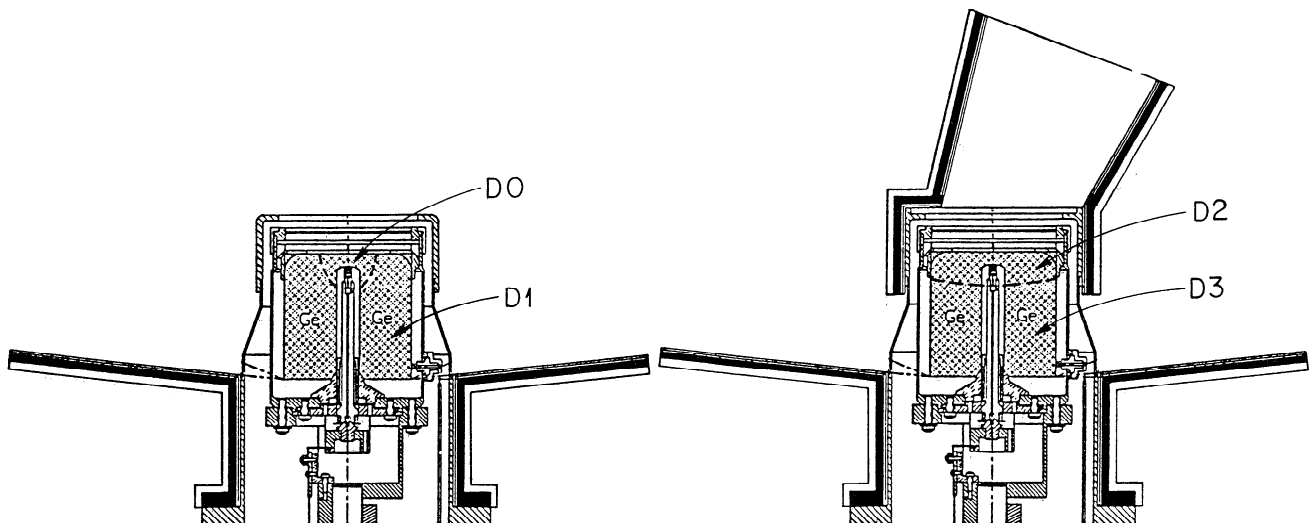The detectors, which are cooled by liquid nitrogen, have an energy resolution of ~2 keV full width at half

Figure 1. Cross section of the coaxial germanium detectors, cryostat, and shielding for the two spectrometers. The left detector rear segment, D1, provided the spectra used here.

maximum (FWHM) up to several hundred keV. Their efficiency is greater than 50% up to about 100 keV for the front segments and 300 keV for the rear segments. Charged cosmic ray particles, which leave many MeV in the detectors, were recorded with an extra electronics chain with much lower gain. While the payload was within line-of-sight of the launch site at Williams Field, every photon and cosmic ray interacting with the detector had its energy (out of 4096 channels) and arrival time (to 50 μs) telemetered directly to the ground station. Out of line-of-sight, 4096-channel spectra were accumulated every 15 min for each detector and recorded on a modified VCR.

Balloon Flight and Data Coverage

The flight, on a 800,000-cubic-meter balloon, was the first circumnavigation of the Antarctic continent by a large balloon payload. Launched by a crew from the National Scientific Balloon Facility (NSBF) on December 21, 1990, at 1850 UT, the payload remained at float altitudes between 37.8 km and 40.2 km with only minimal ballasting for 8.7 days while circling the continent. These altitudes correspond to residual atmospheric depths which never exceeded 4.5 grams/cm^2. The payload was cut down on December 29 upon returning to the Ross Ice Shelf and successfully recovered by U.S. Navy helicopters. The flight path is shown in Fig. 2.

The high albedo of the Antarctic ice produced an additional heat load beyond what the payload was designed to endure, causing the electronics to overheat, resulting in long periods with no data and periods of data at a drastically lowered detector live time ($\sim$1% of

events registered). In all, the 209 hours of flight yielded $\sim$12 hours of data with nearly 100% live time and $\sim$63 additional hours with $\sim$1% live time.

A total of 17 spectra of 15-min accumulation each were obtained during six occasions of precipitation activity. Table 1 summarizes information about these six events. An additional 27 spectra were obtained while the balloon was in the auroral zone (crudely defined as magnetic latitudes between 70° and the lowest latitude reached by the balloon, about 65°) which do not show precipitation. A total of 63 hours of data, both line of sight and accumulated spectra, were obtained while the balloon was over the polar cap region (which includes the launch site). None of the polar cap data show precipitation flux. Due to the thermal problem, only once were we able to observe the onset of a precipitation event (i.e., a 15-min spectrum with no precipitation bremsstrahlung followed by one with significant activity), and we were never able to observe the conclusion of an event.

Each spectrum was tested for precipitation activity by calculating its chi-squared deviation from a typical quiet background spectrum. Using this technique, we could have detected precipitation approximately half as bright as the dimmest event seen (Event 4). Since there are more bright events than dim ones, we are observing a peaked distribution of number versus intensity, rather than a monotonically decreasing distribution.

Data Analysis

The data analysis has four major phases: (1) normalization and background subtraction to obtain a spec-
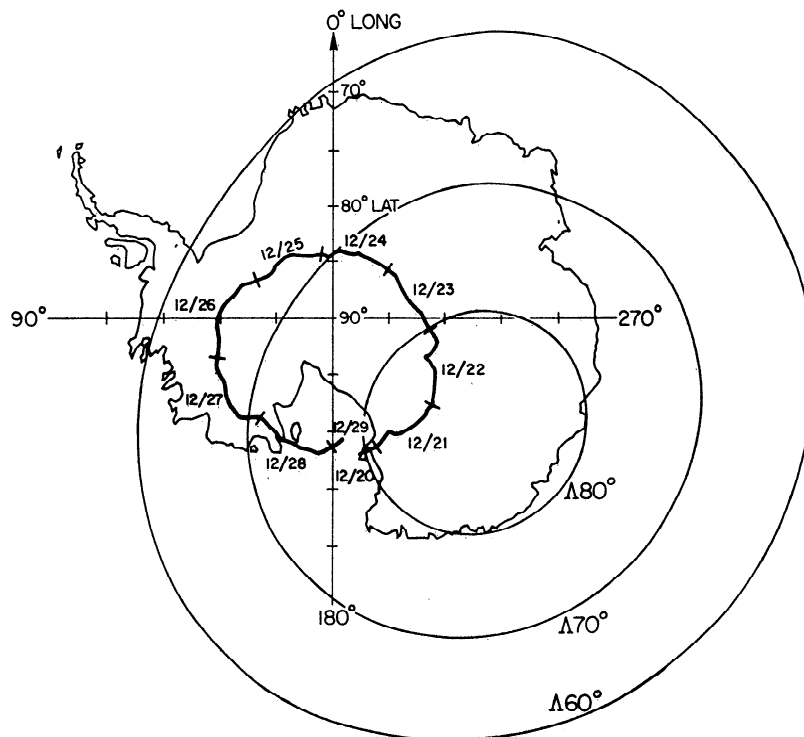

Figure 2. Flight path of the long-duration balloon. The geomagnetic latitude is indicated.

Table 1. Spectra with Precipitation Activity

Event	Day	UT	A, $(\text{cm}^2\,\text{s}\,\text{keV})^{-1}$	E_0,keV	B, keV	C	MLT, hours	L	K_p
1	Dec. 25, 1990	1138	0.38	21.9	31.4	3.3	8.37	6.6	2+
2	Dec. 26, 1990	0402	0.88	35.6	37.2	4.5	23.84	6.0	1-
		0417	0.39	37.4	38.1	4.8	0.12	6.0	1-
		0447	0.63	32.9	37.9	4.6	0.69	6.0	1-
3	Dec. 26, 1990	0711	0.45	29.4	31.3	4.1	3.24	6.0	1
4	Dec. 26, 1990	1830	0.07	44.5	28.6	6.2	13.18	5.7	1-
5	Dec. 26, 1990	2252	0.21	35.9	33.4	5.9	17.12	5.6	1-
	Dec. 27, 1990	0015	0.26	29.0	35.9	2.9	18.45	5.6	1-
		0030	0.37	27.8	37.6	3.8	18.70	5.6	1
		0045	0.40	22.9	37.4	4.7	18.95	5.6	1
		0100	0.50	22.2	43.9	2.8	19.20	5.6	1
6	Dec. 27, 1990	1540	3.5	14.3	26.9	3.0	9.62	7.1	2-
		1555	1.8	15.7	27.0	6.0	9.87	7.1	2-
		1610	3.0	16.8	26.4	4.0	10.12	7.1	2-
		1625	1.7	17.2	31.0	3.3	10.37	7.1	2-
		1640	0.72	18.2	31.6	3.3	10.62	7.1	2-
		1655	0.25	22.3	26.7	3.5	9.87	7.1	2-

trum in units of counts $(\text{cm}^2\,\text{s}\,\text{keV})^{-1}$; (2) removal of the effects of Compton scattering and absorption in the instrument and the atmosphere to obtain a spectrum of the bremsstrahlung in photons $(\text{cm}^2\,\text{s}\,\text{keV})^{-1}$ where it is created; (3) inversion of the bremsstrahlung process to obtain the parent spectrum of the electrons in the atmosphere; and (4) solution of the continuity equation for the slowing down of electrons, to derive the original precipitating spectrum of electrons from the bremsstrahlung-producing spectrum in electrons $(\text{keV}\,\text{s})^{-1}$.

Background Subtraction and Live Time Determination

Comparing raw count spectra with and without bremsstrahlung flux due to precipitation, we see that they
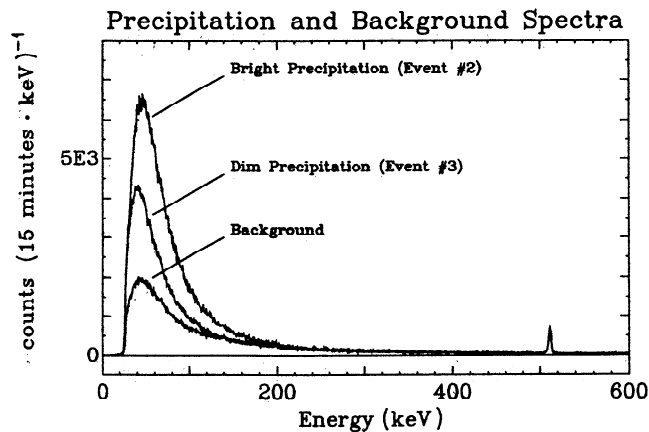

Figure 3. Raw 15-min spectra during times of bright precipitation emission, dimmer (and softer) emission, and quiet background. The narrow background line at 511 keV demonstrates the instrumental resolution.

are identical above ~300 keV (Fig. 3). To derive a spectrum of the bremsstrahlung flux alone, we subtract the standard background spectrum (lowest curve) from each spectrum showing precipitation activity.

Two separate problems involving our knowledge of the detector live times complicated this part of the analysis. First, the thermal problem mentioned above, which reduced the detector live times to ~1% of normal, also left no way of determining the exact live time remaining. Since the variable precipitation flux only occurs at low energies (see Fig. 3), we used the data in the energy range 550-2500 keV to normalize the source spectra to the standard background spectrum in the same detector before subtracting.

The second problem did not vary with time, and was more difficult to discover. At all times during the flight, the overall spectrum in D1 is lower than would be expected by comparison with D3, by about a factor of 2. We have not been able to identify the source of this discrepancy; for the analysis below, we simply use D1 alone. If we were confident that D1 and D3 were consistent, we could use the differing responses of the two detectors versus elevation to estimate the elevation angle of the incoming precipitation flux, and therefore determine its atmospheric correction and distance (see below).

Figure 4 shows six background-subtracted, live-time-normalized count spectra from D1, one from each of the six distinct precipitation events recorded. Variations in intensity and spectral hardness are apparent, as is the degradation in the statistical significance at times when the thermal problem was occurring in the electronics (Events 1, 5, and 6). The smooth curves in Fig. 4 are fits to all of the 15-min precipitation spectra in each event. The fit function is an exponential
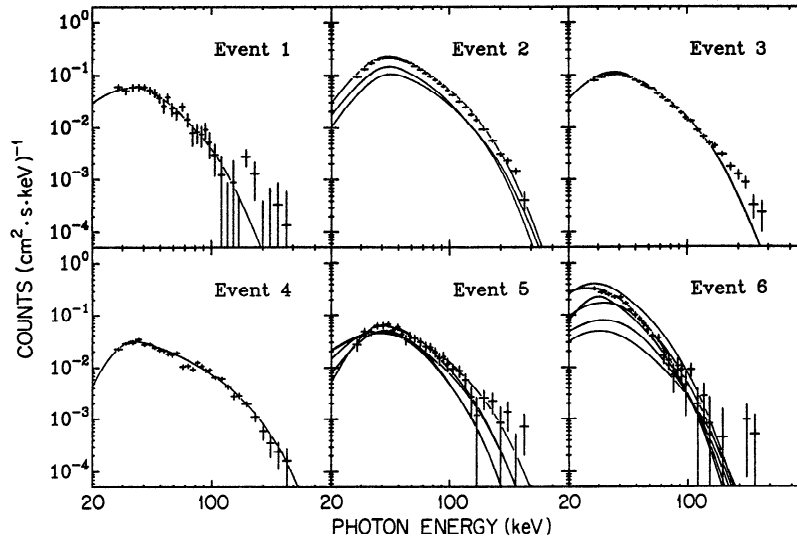
Figure 4. One 15-min, background-subtracted count spectrum from each of the six separate precipitation events observed. Events 2, 3, and 4 were taken with about 100% live time, the rest with near 1% live time. Smooth traces are fits to all spectra; the form of an exponential with low-energy cutoff fits well in all cases.

$A \exp(-E/E_0)$ multiplied by a low-energy cutoff of the form $1 - \exp[-(E/B)^C]$. The parameters A, E_0, B, and C are listed in Table 1.

Removing the Effects of Atmosphere and Instrument

After the background subtraction, the effects of scattering and absorption in the atmosphere and instrument are deconvolved from the data by making use of Monte Carlo simulations of both. Given a particular detector and the balloon's atmospheric depth, the only additional piece of information needed to complete the deconvolution is the elevation angle above the horizon of the precipitation activity. Previous analyses of similar balloon data [e.g., *Anderson and Enemark*, 1960] have proceeded by assuming the precipitation to be occurring over the whole sky at once. We will demonstrate our analysis both under this assumption and under the assumption that the precipitation takes place at a single elevation angle, either 15° or 30°.

The instrumental Monte Carlo simulation includes 19 regions of material for D1 (no collimator), including the germanium itself, aluminum and plastic cryostat pieces, and lead, tin, and copper shielding. Nearly every piece visible in Fig. 1 is reproduced to ~1-mm accuracy. Photons are input with varying elevation angle and energy. The output is a set of response matrices, that is, simulated count spectra as a function of original angle and energy. The solid trace in Fig. 5 shows one such count spectrum, for photons initially between 100 and 110 keV entering D1 at 30° from the horizontal.

Another set of matrices is obtained for the atmosphere by a simulation of 10 concentric shells of air with different heights and densities representing the entire atmosphere of the Earth. Photons are started isotropically from a single point 80 km above the Earth's surface (although the electrons of a few keV which are respon-

sible for aurorae stop at around 100 km, electrons on the order of 100 keV penetrate to about 77 km [*Berger and Seltzer*, 1972]). When the simulated photons reach atmospheric depths typical of the balloon flight (3.5 and 4.5 g/cm²), their current angles and energies are recorded, resulting in sets of spectra at these altitudes as a function of initial photon energy, initial photon angle, and final photon angle.

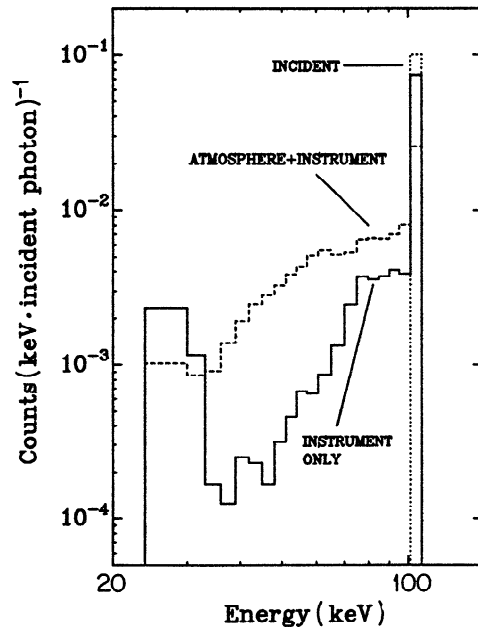The effects of Compton scattering and absorption in the atmosphere on photon spectra have been addressed

Figure 5. Response to incident photons in the energy range 100-110 keV at an elevation angle of 30°. (solid line) Detector response only. (dashed line) Combined response of the atmosphere and the detector. (dotted line) Monoenergetic input spectrum.
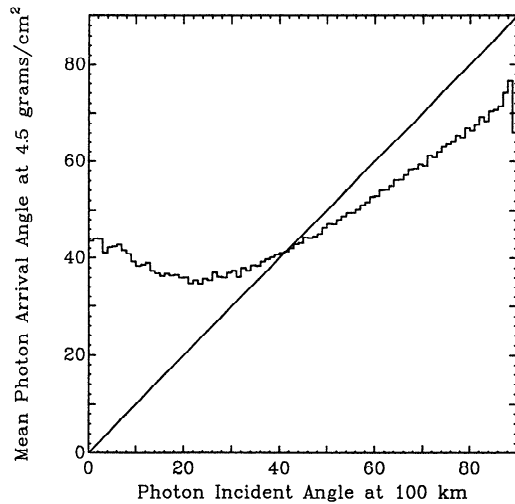
Figure 6. Distortion of the apparent elevation of a precipitation event by the atmosphere. (diagonal line) No atmosphere (photon arrival angle equals the initial photon angle). (irregular line) Apparent mean elevation of photons at 4.5 g/cm^2 atmospheric depth.

by other authors [e.g., *Berger and Seltzer*, 1972]. In addition to this spectral effect, we have now simulated the effect on the angular distribution of the radiation as well. Figure 6 illustrates the mean elevation angle of the photons arriving at balloon altitude versus what they would have been in the absence of the atmosphere. The high absorption at low initial angles means that the only photons which survive from events near the horizon are those which scatter early on to steeper elevation angles. The lowest events therefore appear to be coming from higher up; indeed, there is a minimum apparent elevation of about 35° (for an initial elevation of about 20°).

The instrumental and atmospheric matrices are combined by multiplying and summing terms so that the final response matrix gives count spectra in the detector as a function of original photon energy and original angle. The dotted line in Fig. 5 is a count spectrum with the same initial parameters that produced the solid line, but with the effects of 4.5 g/cm^2 of atmosphere on photon angles and energies included.

Given the final response matrices, there are two ways to apply them to the data. In the first method, "forward folding," a number of possible input photon spectra can be multiplied by the response matrix to give hypothetical count spectra. The photon spectrum corresponding to the count spectrum which best fits the data is taken to be the actual original photon spectrum. This method, long used for hard X-ray and gamma-ray spectra from scintillators, is known to be "forgiving" in that input spectra of many forms can often fit the same final count spectrum well.

The method we use here, "direct inversion," is mathematically equivalent to multiplying the count spectrum by the inverse of the response matrix to get a unique incident photon spectrum. It is suitable for spectra from germanium detectors, in which the width of the energy

bins under consideration is generally much greater than the detector resolution. This assures that a photon in one energy bin will produce counts only in equal or lower bins (i.e., the response matrix is triangular). The direct inversion method and other restrictions on it are discussed by *Johns and Lin* [1992] and by *Smith et al.* [1993].

The top panels of Fig. 7 show the X-ray count spectrum from Event 3 of Fig. 4 (lower set of data points) along with the photon spectrum obtained by directly inverting the atmospheric and instrumental response matrix (upper set of data points). In the left panel the assumed elevation angle is 15°; in the center panel it is 30°; in the right panel the precipitation is assumed to occur evenly across the whole sky. Elevations above ∼45° are ruled out because all the precipitation events were observed at comparable count rates in D3 and D1, and D3 is shielded from high elevation angles.

Derivation of X-Ray-Producing Electron Spectra

We would like to compare our bremsstrahlung results to the many in situ measurements of precipitating electron fluxes by satellites. Our instrument, however, is sensing these electrons remotely and integrating the emission coming from a region of unknown area. The photon spectra derived above is in photons $(cm^2\,s\,keV)^{-1}$ at the detector. To convert properly to a photon flux at the point of origin, we would have to multiply by the area of a sphere with radius equal to the distance between the source region and the detector and then divide by the area of the source region. The distance would be known if we knew the approximate elevation angle, but the area is not known at all.

Given the photon spectrum (Fig. 7, top panels), we can derive the corresponding parent electron spectrum (Fig. 7, bottom panels) by the method of *Johns and Lin* [1992]. In this technique, a response matrix is calculated for the bremsstrahlung process and inverted directly just as the atmosphere-plus-detector response matrix was above. The bremsstrahlung matrix is much more strongly nondiagonal, however, so the errors on the inverted spectrum are much higher. The data are therefore accumulated into larger energy bins to improve the statistics. The photon spectrum is extrapolated to higher energies (using the power law defined by the highest two data points) to calculate the electron spectrum at the highest energies.

The bremsstrahlung cross sections, integrated over angle, are taken from *Koch and Motz* [1959]: below 80 keV the Bethe-Heitler formula in the nonrelativistic limit with the Elwert correction joined smoothly between electron energies of 80 and 120 keV with the relativistic form of the Bethe-Heitler formula. In the energy range 20-300 keV these cross sections should be accurate to 10-20% [*Koch and Motz*, 1959].

The X-ray-producing electron spectra are shown as the lower spectra in the bottom panels in Fig. 7.

Conversion to Precipitating Electron Spectra

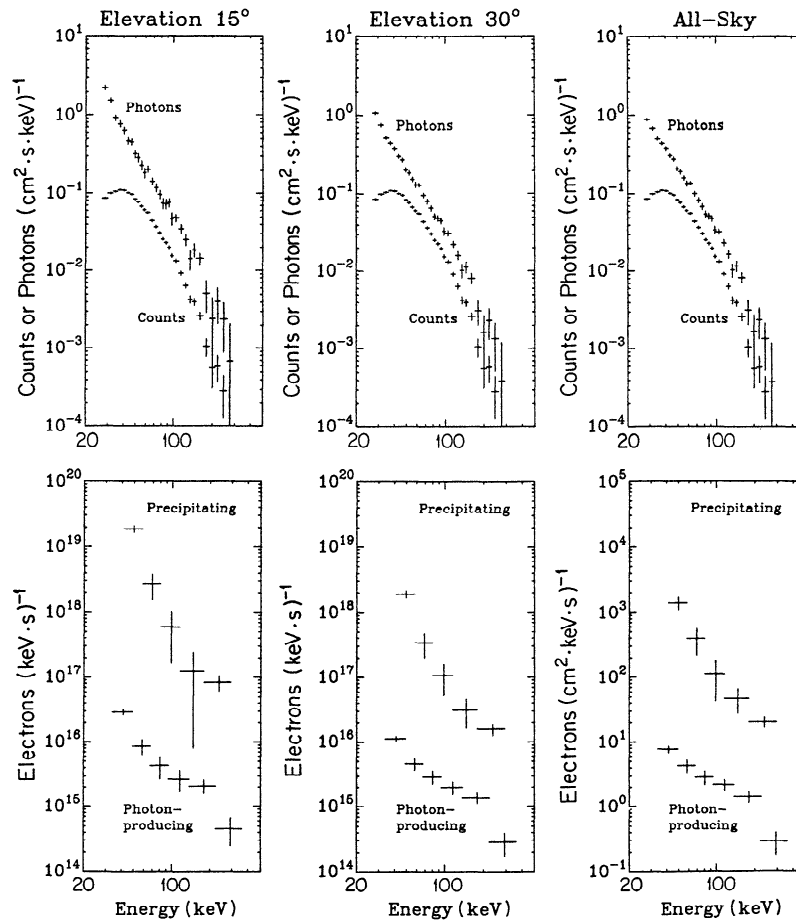The spectrum of X-ray-producing electrons includes some which have already lost part of their energy to

Figure 7. The top panels show X-ray spectra: bottom trace is count spectrum (same as Fig. 4, Event 3); top trace is deconvolved photon spectrum. The bottom panels on the right show deconvolved electron spectra; lower points are photon producing electrons; upper points are precipitating electrons. The left panels are for assumed source elevation of 15°; the middle panels for assumed source elevation of 30°; and the right panels for precipitation assumed uniform on the sky.

ionization and excitation of air. To convert this X-ray-producing electron spectrum to the spectrum of precipitating electron at the top of the atmosphere, we use a continuity equation which relates the input spectrum, total instantaneous spectrum, and energy loss rate for the electrons [*Johns and Lin*, 1992]. We assume that the precipitating electron spectrum varies slowly compared to the stopping time of an electron in the atmosphere. The steady state continuity equation is then

$$(E) \; = \; \frac{d}{dE}\left(N(E)\frac{dE}{dt}\right) \tag{1}$$

where $F(E)$ is the precipitating spectrum in electrons $(\text{keV s})^{-1}$, $N(E)$ is the bremsstrahlung-producing electron population in electrons/keV, and dE/dt is the energy loss rate of an electron, also a function of energy. We assume that Coulomb collisions dominate the electron energy loss process and use the Bethe-Bloch formula [see *Jackson*, 1975, p.269] for dE/dx and multiply by electron velocity to get dE/dt. The precipitating electron spectra are shown as the upper spectra in the bottom panels of Fig. 7. Note that in the rightmost panels of Fig. 7, where we assume the precipitation

occurs over the whole sky, the derived electron spectrum is in electrons $(\text{cm}^2\,\text{s}\,\text{keV})^{-1}$ rather than electrons $(\text{keV s})^{-1}$.

Frequency of Occurrence and Location of Precipitation

Since K_p was low (1- to 2+) during all our precipitation times, the results we obtain below should be taken as typical of quiet time. As mentioned above, there are a number of bright precipitation spectra and a number with no observable flux, and only one (Event 4) with a faint flux near our detection limit. We can therefore divide the observations into two distinct sets, with precipitation on and off.

Only for Event 1 do we actually see a transition between the two states, in this case the turn on of precipitation. All the other transitions are hidden by data gaps. For Event 1, however, $K_p = 2+$, the highest of the six precipitation events, and South Pole station riometer and magnetometer records show evidence suggesting a small substorm beginning at ∼1130 UT (T. Rosenberg, private communication, 1991).
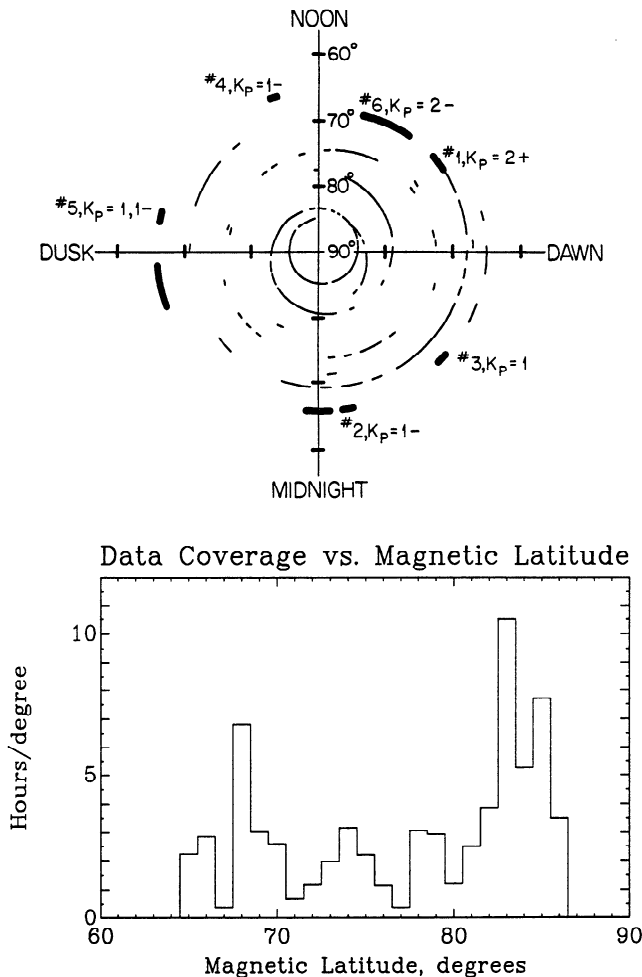
Figure 8 (top) shows the balloon's position, during

NOON

Data Coverage vs. Magnetic Latitude

Figure 8. (top) The spiral track of the balloon in coordinates of magnetic latitude (radius) and magnetic local time (angle). Times for which data are available are shown by a thin line; times when the data show precipitation flux are shown by a thick line and labeled to correspond with the event numbering in Fig. 4 and Table 1. Events 2 and 5 are interupted by data gaps. (bottom) Histogram of available data as a function of magnetic latitude.

times when usable data were obtained, in coordinates of magnetic latitude and magnetic local time, referenced to a magnetic dipole pole at -74.35° latitude, 121.0° east longitude. The heavy lines indicate times with precipitation activity, and the thin lines indicate times when precipitation activity was either absent or much less than the continuous background due to cosmic ray interactions with the atmosphere. The six precipitation events from Fig. 4 are labeled in the figure.

All six events occur within about 2° of the trapping boundary for electrons >300 keV, which we determined with data from the NOAA 10 satellite (H. Sauer, private communication, 1991) for the week of our flight. Both the day-to-day variation of the boundary and the uncertainty of the position of the precipitation relative to the balloon's position give errors of about 2°, so all precipitation events are consistent with this boundary. The >30 keV boundary is 0° to 10° higher in latitude

than the >300 keV boundary, depending on the magnetic local time, so the events are generally within the trapped zone for >30 keV electrons. The spectral variation among these events is discussed in the following section.

Clustering of electron precipitation near the trapping boundary was observed in a much larger sample of events by the OGO 4 satellite [Brown and Stone, 1972]. The duty cycle of precipitation in the auroral zone ($\sim$16 out of 44 spectra) is comparable to the result of Anderson and Enemark [1960], who found a duty cycle of 40% in the northern auroral zone, at values of K_p between 1 and 4.

High-energy precipitation has been observed to occur occasionally at invariant latitude $\sim$ 75° (South Pole station) in early afternoon, local time [Matthews et al., 1988]. Taking magnetic latitude as equivalent to invariant latitude (which is accurate to about 1° over our flight path), we see from Fig. 8 (bottom) that we have about 10 hours of data within 2° of this latitude, none of which show any precipitation. At even higher latitudes, connected to open field lines at all times of day, precipitation is known to be infrequent, as has been demonstrated by a number of polar satellites [O'Brien, 1962, 1964; Brown and Stone, 1972; Imhof et al., 1990].

Spectral Variation of Precipitation

It has been frequently observed that the boundary of electron trapping is at higher latitudes for lower energy electrons. Since electron precipitation generally begins at this boundary, the mean energy of precipitated electrons increases with decreasing latitude [e.g., Imhof et al., 1979, 1991]. Thus the auroral zone, defined by visible glow caused by electrons of a few keV, is at about L=7.8, while the maximum precipitation > 40 keV is at about L=5-6 [O'Brien, 1964]. This effect was observed in the trapping boundaries for electrons >30 keV, >100 keV, and >300 keV at the time of our flight (H. Sauer, private communication, 1991) and can be seen in Fig. 9a, where the best-fit exponential scale energy E_o is plotted as a function of L for all the precipitation spectra we obtained. Because most of the spectra did not have adequate statistics to apply the inversion techniques described above, E_o is derived directly from the count spectra and is taken from the fits of Fig. 4 (see Table 1).

The dependence of the spectral hardness and other precipitation characteristics on magnetic local time is much more complicated [Barcus and Rosenberg, 1966; Brown, 1966], but in general the typical nighttime or dawn event is found to be softer than the typical daytime event, and more likely to be correlated with magnetic activity. This correlation is not visible when E_o is plotted versus magnetic local time for our events (Fig. 9b). Instead, the softest events occur just before noon, and the hardest near midnight. Considering the small size of the sample, the correlation with L, and the fact that events with a broad range of hardness and flux have been observed at one time or another at all magnetic times, this should not be surprising.
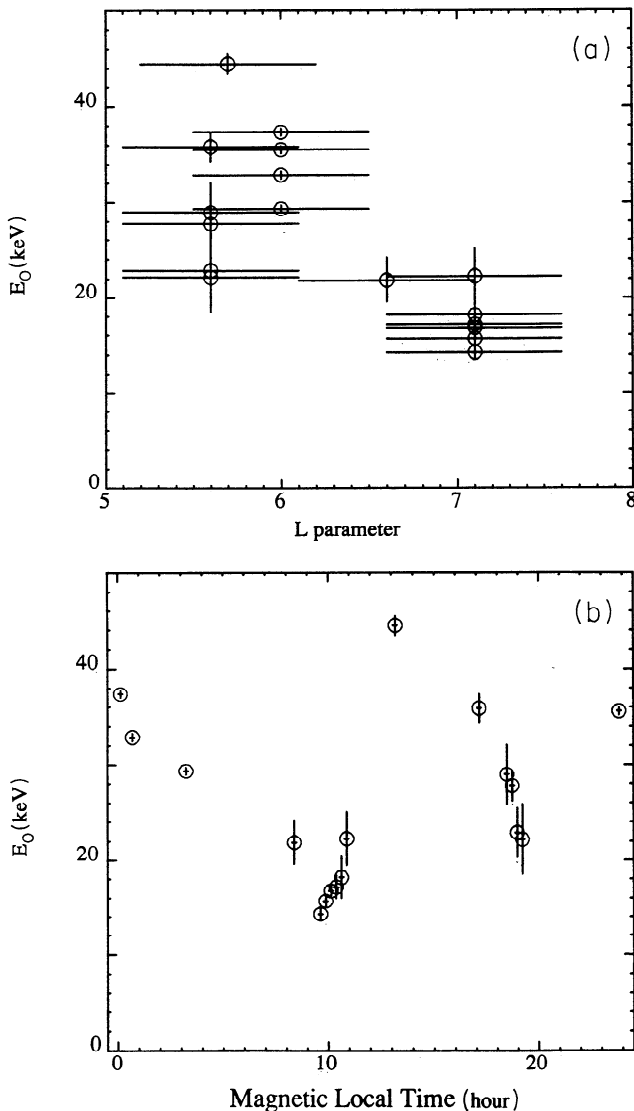
Figure 9. Dependence of the exponential scale-energy fit to the count spectra as a function of (a) McIlwain L parameter and (b) magnetic local time.

A small amount of riometer absorption activity at 30 MHz (not far above the background variability) was observed at South Pole station (far from the balloon) during Event 1 (1130 UT, December 25, 1990) and Event 6 (1630 UT, December 27, 1990). Event 6 was both the brightest and the softest we observed, and Event 1, though not bright, was the next softest and closest to Event 6 in magnetic local time (8 hours versus 9-10 hours for Event 6). Perhaps the softer events also included a bright, even softer component at energies too low for us to observe, which contributed most of the precipitated energy. Exponential distributions at energies of a few keV are common [e.g., *Datlowe et al.*, 1988; *Vij et al.*, 1975] and spectra with two exponential components, hard and soft, have also been observed [*Christensen and Karas*, 1970].

Event 1 is the only event where the onset is observed, that is, in adjacent 15-min spectra the X-ray spectra went from background to a detectable precipitation flux. As indicated earlier, an increase in riometer ab-

sorption was observed at South Pole station beginning near 1130 UT on December 25, as well as variations in the magnetic field (T. Rosenberg, private comunication, 1991). Thus there is the possibility that a small substorm may have begun at that time, leading to the observed precipitation.

Total Rate of Precipitation

The >20 keV X-ray count rates we observe above background range from 1.6 to 12 counts $cm^{-2} s^{-1}$. When compared to other uncollimated detectors flown at auroral altitudes [e.g., *Anderson et al.*, 1965], these levels are comparable to typical background or "drizzle" from the trapped radiation and about an order of magnitude less than substorm levels.

O'Brien [1962] calculated the time that would be required to drain a given flux tube of trapped radiation given observed precipitation rates. *Parks* [1970] applied this technique to precipitation observed during substorms to demonstrate that the time to drain a flux tube was much less than the time to refill it by gradient drift of electrons in longitude (using a drift period of 6000s). He therefore concluded that the electrons must be accelerated promptly in the flux tube from which they precipitate. Looking at relativistic (> 1 MeV) electrons, *Sheldon* [1991] modelled quiet-time auroral-zone precipitation as a combination of processes which do not involve fresh acceleration of energetic particles: pitch angle diffusion into the drift loss cone and wave-particle interactions from lightning or VLF noise.

O'Brien [1962] gives the formula for the time to drain a flux tube as

$$\tau = \frac{0.1 L^4 J_0}{D} \text{ s,} \qquad (2)$$

where L is the McIlwain parameter, J_0 the omnidirectional trapped electron flux in $(cm^2 sec)^{-1}$ at the Earth's equator, and D the precipitating electron flux in $(cm^2 sec)^{-1}$, both fluxes integrated above 40 keV.

As mentioned above, our detectors integrate X-rays from precipitation over the sky, without imaging of the X-rays, the precipitation area is unknown. *Parks et al.* [1994] flew a hard X-ray pinhole camera aboard our Antarctic balloon payload which recorded an image of one precipitation event during the flight, near the time of Event 1 (see Fig. 4). This imaged patch of precipitation was about 30 km across, giving an area of about $7 \times 10^{12} cm^2$. No simultaneous observations with the two instruments, however, were obtained.

The draining time for a single spectrum (that of Event 3, which is shown in Fig. 7) is calculated under the three assumptions in that figure: precipitation in a 30-km diameter patch at an elevation of 15°, at 30°, and over the whole sky (defined as elevations from 10-90°). The last will be the lower limit to the possible electron precipitation per square centimeter, since the precipitation is spread over the maximum possible area. This event occured at $L = 6.0$ at a time when $K_p = 1$. The precipitating flux > 40 keV calculated by integrating the spectra in the bottom panels in Fig. 7 is 1.4 $\times 10^{20}$

electrons/s, 4.7×10^{19} electrons/s, and 4.2×10^4 electrons $(cm^2 s)^{-1}$, from left to right. Dividing the first two by the area seen by *Parks et al.* [1994] gives 1.9×10^7 electrons$(cm^2 s)^{-1}$ and 6.7×10^6 electrons $(cm^2 s)^{-1}$ for 15° and 30° elevation. For an equatorial measurement of average trapped electron flux, we use the > 40 keV electron flux from Explorer 12 which *O'Brien* [1962] used originally: 5×10^6 electrons $(cm^2 s)^{-1}$ from about $L=3.1$ to 8.5.

Using these numbers, we find draining times of 34 s, 96 s, and 15,400 s for the three electron spectra of Fig. 7, reading top to bottom. The two which assume a 30-km diameter patch are much faster than the 6000-s timescale for replenishing the flux tube by longitudinal drift, and also much faster than the average draining time of 20,000 s calculated by *O'Brien* [1962] for geomagnetically quiet times at similar values of L.

We have summed all 44 background-subtracted spectra from magnetic latitudes of 65-70° (28 of which were essentially zero) and inverted this average spectrum in the manner shown in Fig. 7 for a single spectrum to obtain the average precipitation flux over the flight. We use the inversion for precipitation uniform on the sky, which gives an average precipitation of 3.6×10^{19} electrons/s. We do not mean to imply in this case that the precipitation occurs over the entire sky, merely that there may be many patches at many different elevations contributing to this averaged spectrum. Using the equation above, we find that this flux would have to be spread over an area of 9×10^{14} cm^2, or a patch 340 km in diameter in order to reproduce a 20,000-s draining time. This is almost the entire sky viewed from the balloon.

Therefore, if the electron precipitation covers anything less than the full sky, we would conclude that quiet-time precipitation, like the substorm precipitation studied by *Parks* [1970], must contain freshly accelerated electrons.

Conclusions

Bremsstrahlung spectra from electron precipitation in the auroral zone have been measured with an unprecedented combination of high spectral resolution and sensitivity up to the apparent cutoff of the flux at $\sim$300 keV. The ad hoc exponential law usually used to model the precipitating electron spectra is shown to agree well with observations at very high sensitivity (see Fig. 4). The frequency of events, their distribution in geomagnetic coordinates (consistent with the trapping boundary), and the dependence of spectral hardness on L are consistent with previous surveys from balloons and satellites. If this quiet-time precipitation is occurring in small ($\sim$30 km) patches like that observed by *Parks et. al.* [1994] during this flight and not uniformly over essentially the entire sky, then the implied precipitation fluxes per unit area would require freshly accelerated electrons. Similarly, if we assume that the fluxes per unit area are similar to those average fluxes measured by *O'Brien* [1962] for geomagnetically quiet times, we

can conclude that the precipitation must be occurring over very large areas (i.e., patches a few hundred kilometers across) in order to produce the bright photon fluxes we observe.

We have shown that a large sample of bright, quiet-time precipitation events can be observed by an unshielded germanium detector on a long-duration balloon flown in Antarctica. We have demonstrated methods of model-independent compensation for the effects of the bremsstrahlung process, atmospheric scattering and absorption, and instrument response. The addition of imaging information over the whole sky to determine the elevation and area of precipitation patches would allow accurate, model-independent measurements of the spectrum and intensity of precipitating electrons.

References

Anderson, K. A., Balloon observations of X-rays in the auroral zone, I, *J. Geophys. Res.*, *65*, 551, 1960.

Anderson, K. A., Balloon measurements of X-rays in the auroral zone, in *Auroral Phenomena*, edited by M. Walt, p. 46, Stanford Univ. Press, Stanford, Calif., 1965.

Anderson, K. A., and D. E. Enemark, Balloon observations of X-rays in the auroral zone, II, *J. Geophys. Res.*, *65*, 3521, 1960.

Barcus, J. R., and T. J. Rosenberg, Energy spectrum for auroral-zone X-rays, 1, Diurnal and type effects, *J. Geophys. Res.*, *71*, 803, 1966.

Berger, M. J., and S. M. Seltzer, Bremsstrahlung in the atmosphere, *J. Atmos. Terr. Phys.*, *34*, 85, 1972.

Brown, J. W., and E. C. Stone, High-energy electron spikes at high latitudes, *J. Geophys. Res.*, *77*, 3384, 1972.

Brown, R. R., Balloon observations of auroral X-rays, *J. Geophys. Res.*, *66*, 1379, 1961.

Brown, R. R., Electron precipitation in the auroral zone, *Space Sci. Rev.*, *5*, 335, 1966.

Brown, R. R., and J. R. Barcus, Balloon observations of the extent and structure of auroral-zone electron precipitation events, *J. Geophys. Res.*, *68*, 6069, 1963.

Christensen, A. B., and R. Karas, Energy spectra of precipitating electrons from observations of optical aurora, bremsstrahlung X-rays, and auroral absorption, *J. Geophys. Res.*, *75*, 4266, 1970.

Datlowe, D. W., W. L. Imhof, and H. D. Voss, X-ray spectral images of energetic electrons precipitating in the auroral zone, *J. Geophys. Res.*, *93*, 8662, 1988.

Imhof, W. L., J. B. Reagan, and E. E. Gaines, Studies of the sharply defined L dependent energy threshold for isotropy at the midnight trapping boundary, *J. Geophys. Res.*, *84*, 6371, 1979.

Imhof, W. L., J. Mobilia, D. W. Datlowe, H. D. Voss, and E. E. Gaines, Longitude and temporal variations of energetic electron precipitation near the trapping boundary, *J. Geophys. Res.*, *95*, 3829, 1990.

Imhof, W. L., H. D. Voss, J. Mobilia, D. W. Datlowe, and E. E. Gaines, The precipitation of relativistic electrons near the trapping boundary, *J. Geophys. Res.*, *96*, 5619, 1991.

Jackson, J. D., *Classical Electrodynamics*, John Wiley & Sons, New York, 1975.

Johns, C. M., and R. P. Lin, The derivation of parent electron spectra from bremsstrahlung hard X-ray spectra, *Solar Phys.*, *137*, 121, 1992. (Erratum, *Solar Phys.*, *142*, 219, 1992.)

Koch, H. W., and J. W. Motz, Bremsstrahlung cross-section formulas and related data *Rev. Mod. Phys.*, *31*, 920, 1959.

Matthews, D. L., T. J. Rosenberg, J. R. Benbrook, and E. A. Bering III, Dayside energetic electron precipitation over the South Pole (lambda=75°), *J. Geophys. Res.*, *93*, 12941, 1988.

O'Brien, B. J., Lifetimes of outer-zone electrons and their precipitation into the atmosphere, *J. Geophys. Res.*, *67*, 3687, 1962.

O'Brien, B. J., High-latitude geophysical studies with satellite Injun 3, 3, Precipitation of electrons into the atmosphere, *J. Geophys. Res.*, *69*, 13, 1964.

Parks, G. K., The acceleration and precipitation of Van Allen outer zone energetic electrons, *J. Geophys. Res.*, *75*, 3802, 1970.

Parks, G. K., T. Freeman, M. McCarthy, and S. Werden, Images and energy spectra of an impulsive X-ray burst observed in the Antarctic polar cap region, *Antarct. J.*, *5*, 301, 1994.

Sheldon, W. R., On the precipitation of relativistic electrons from the outer belt, *J. Atmos. Terr. Phys.*, *53*, 17, 1991.

Smith, D. M., *et al.*, Compton-backscattered annihilation radiation from the galactic center region, *Astrophys. J.*, *414*, 165, 1993.

Vij, K. K., D. Venkatesan, W. R. Sheldon, J. W. Kern, J. R. Benbrook, and B. A. Whalen, Simultaneous investigation of parent electrons and bremsstrahlung X-rays by rocket-borne detectors, *J. Geophys. Res.*, *80*, 2869, 1975.

Winkler, J. R., L. Peterson, R. Arnoldy, and R. Hoffman, X-rays from visible aurorae at Minneapolis, *Phys. Rev.*, *110*, 1221, 1958.

K. A. Anderson, K. Hurley, and R. P. Lin, Space Sciences Laboratory, University of California, Berkeley, CA 94720. (e-mail: boblin@sunspot.ssl.berkeley.edu).

C. M. Johns, McDonald Observatory, University of Texas, Austin, TX, 78712.

D. M. Smith, Astronomy Department, University of Maryland, College Park, MD 20742.